Free Radical Biology and Medicine 108 (2017) 118–128

Contents lists available at ScienceDirect

Free Radical Biology and Medicine

journal homepage: www.elsevier.com/locate/freeradbiomed

Original article

Ultraviolet A-induced oxidation in cornea: Characterization of the early oxidation-related events

Corinne Zinflou[a,b], Patrick J. Rochette[a,b,c,*]

[a] Axe Médecine Régénératrice, Centre de Recherche du CHU de Québec – Université Laval, Hôpital du Saint-Sacrement, Québec, QC, Canada
[b] Centre de Recherche en Organogénèse Expérimentale de l'Université Laval/LOEX, Université Laval, Québec, QC, Canada
[c] Département d'Ophtalmologie et ORL - chirurgie cervico-faciale, Université Laval, Québec, QC, Canada

ARTICLE INFO

Keywords:
UVA
Cornea
Oxidative stress
Reduced pyridine nucleotides
Oxidized mitochondrial flavins
8-OHdG
Glutathionylated proteins

ABSTRACT

Exposure to sunlight ultraviolet-A (UVA), the main component of solar UV reaching the eyes, is suspected to play an important part in the onset of ocular pathologies. UVA primary biological deleterious effects arise from the photo-induction of oxidative stress in cells. However, the molecular bases linking UVA-induced oxidation to UVA toxicity in eyes remain poorly understood, especially with regards to the cornea. To shed some light on this issue, we have investigated the susceptibility and response potential of the different corneal cellular layers (epithelium, stroma and endothelium) to UVA-induced oxidation. We have monitored UVA-induced immediate effects on cellular redox balance, on mitochondrial membrane potential, on 8-Hydroxy-2′-deoxyguanosine (8-OHdG) accumulation in cellular DNA and on S-glutathionylated proteins (PSSG) levels along whole rabbit corneas. Higher redox imbalance was observed in the posterior part of the cornea following irradiation. Conversely, UVA-altered mitochondrial membrane potentials were observed only in anterior portions of the cornea. UVA-induced 8-OHdG were found in nuclear DNA of epithelia, while they were found in both nuclear and mitochondrial DNA in stromal and endothelial cells. Finally, significantly higher levels of cytosolic PSSG were measured in epithelia and endothelia immediately after UVA exposure, but not in stromas. Taken together, our findings indicate that while corneal epithelial cells are subjected to important modifications in response to UVA exposure, they efficiently limit the early manifestations of UVA-induced toxicity. On the other hand, the corneal endothelium is more susceptible to UVA-induced oxidation-related toxicity.

1. Introduction

Ultraviolet light (UV) is the most energetic radiations of the solar spectrum that reaches the human eyes. Shorter solar UV wavelengths affecting the eyes (long UVB; 290–315 nm) are essentially absorbed by the cornea and the lens cortex [1,2]. The cornea also absorbs around 35% of the light in the UVA range (315–400 nm). The fraction passing through the cornea is transmitted to the lens nucleus, where it is absorbed [1,3]. As high-energy photon radiation implies a strong biological damage potential in absorbing tissues, exposure to UV light represents a health hazard. Indeed, exposure to UV rays is a proven risk in many ocular diseases including photoconjunctivitis, pterygium, climatic droplet keratopathy, photokeratitis and cataracts [4–6]. Since UVA wavelengths represent ~95% of the incident solar UV radiations, they are suspected to play an important part in the onset of these pathologies, but might also affect eyes proper functioning.

It is well documented that UVA exposure has deleterious effects that could promote photo-aging [7,8], trigger cell malignant transformation [9,10] or drive tumor progression [11] in skin. But in the eye, UVA molecular consequences have been less often addressed. Proteins aggregation [12] and alterations in signal transduction [13], gene expression [14,15] or cell metabolism profile [16–18] are among UVA-induced disturbances reported in ocular structures. However, research efforts have been focused mainly on the impact of UVA exposure on the lens [13,15,19,20], with little emphasis to the cornea.

UVA primary biological toxicity arises from the photo-production of reactive oxygen species (ROS) [21–24]. ROS formation is mediated by UVA-excited endogenous chromophores that act on molecular targets through type I or II photosensitization reactions. UVA exposure can increase cellular ROS levels above the antioxidant buffering capacity, thereby disrupting reduction-oxidation (redox) homeostasis and exposing the cells to an oxidative stress. Excessive ROS levels rapidly result in oxidative damage to proteins, cellular membranes, mitochondrial and/or nuclear DNA. Besides, mitochondria highly depend on redox processes for their functions, biogenesis and turnover [25]. They exist as a dynamic network in cells, modulating death, signal transduction,

* Corresponding author at: Axe Médecine Régénératrice, Centre de Recherche du CHU de Québec – Université Laval, Hôpital du Saint-Sacrement, Québec, QC, Canada.
E-mail address: Patrick.rochette@orlo.ulaval.ca (P.J. Rochette).

http://dx.doi.org/10.1016/j.freeradbiomed.2017.03.022
Received 21 November 2016; Received in revised form 8 March 2017; Accepted 20 March 2017
Available online 22 March 2017

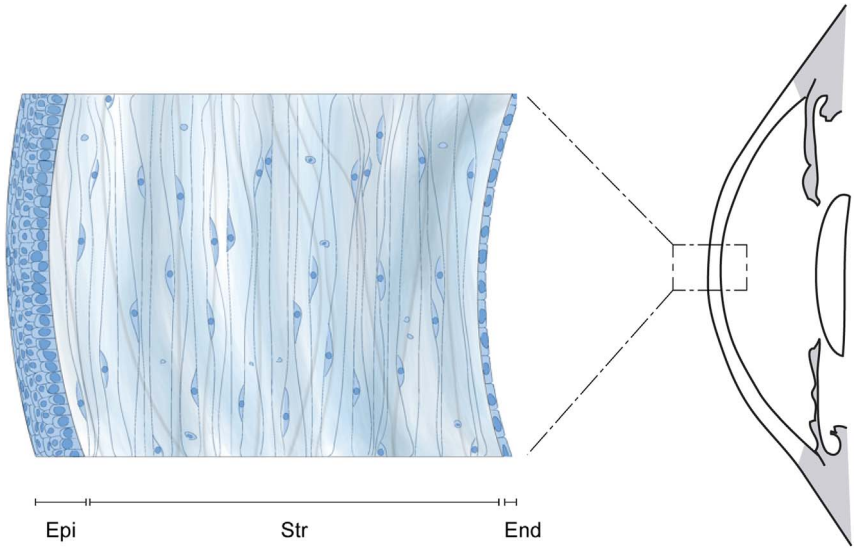

Fig. 1. Cornea anatomy. Schematic representation of the cornea with its three cellular layers (from outer to inner eye): epithelium, stroma and endothelium. Epi: epithelium, Str: stroma End: endothelium.

cell growth and differentiation [25,26]. In order to maintain homeostasis and proper mitochondrial activities under challenging conditions, redox-active components modulate antioxidant systems. These systems regulate ROS flux and amplify and/or trigger a set of signaling pathways that control survival, proliferation or cell death. These components included proteins with redox-sensitive amino acids being reversibly oxidized under stress. Crucial reactive cysteine and methionine residues are the most frequent reversibly altered residues of redox-responsive proteins [27]. Determining the distribution profile of early macromolecular alterations, such as oxidative damage to cell components and redox-active proteins modifications, is necessary to understand the molecular basis of tissues response to UVA-induced oxidation. It could help characterize the oxidation-related events that foster tissue dysfunctions/failure after UVA exposure and identify precisely the UVA toxicity sensitivity of different ocular structures.

The cornea shields inner ocular structures against UVA. It contains three major cellular layers (Fig. 1), each harboring different properties. From anterior to posterior, the cornea is composed of a multi-layered self-renewal epithelium with highly proliferative cells; a stroma containing quiescent fibroblastic-like cells; and a mono-layered endothelium with highly metabolically active post-mitotic cells. So far, very little is known on UVA-induced toxicity mechanisms in the cornea. In fact, only a few studies have recently investigated the molecular consequences of UVA exposure on corneal cells or whole corneas [16,28–31]. These consequences include effects on cytokines profiles expression in limbal corneal stem cells and fibroblasts [16], on transcriptomic and proteomic patterns in corneal stroma [29], on matrix metalloproteinase expression in corneal epithelium [30] and on corneal metabolic rate [31]. Besides, the initial steps linking UVA exposure of cornea to the reported effects still remain poorly understood.

We thus aimed to characterize the early macromolecular alterations occurring in the cornea after an exposure of whole rabbit eyes to UVA rays. Using “oxidized mitochondrial flavins” ($^{ox}Fv_m$) to “reduced pyridine nucleotides” (NAD(P)H) fluorescence signal ratio measurement as an indicator of the redox environment, we monitored UVA-induced immediate changes in cellular redox balance as a function of corneal depth, in corneal epithelium, stroma and endothelium. Indeed, variations in that balance reflect the extent of UVA-induced oxidation in view of the tissue anti-oxidant capacity. We then proceeded to an examination of mitochondrial membrane potential variations in the three corneal layers. Afterward, we investigated the extent and distribution of UVA-induced oxidative-related molecular alterations in the cornea. More precisely we investigated the occurrence of 8-Hydroxy-2′-deoxyguanosine (8-OHdG) accumulation, the preeminent UVA-induced oxidative DNA lesion [32], in mitochondria and nuclei. We also assessed UVA-induced alterations of redox-active proteins. This was achieved using the level of S-glutathionylated proteins (PSSG) as an indicator of critical-cysteine-containing proteins oxidation. Proteins S-glutathionylation is a glutathione-dependent modification that targets cysteine residues. It results in the reversible formation of mixed disulfide bonds between proteins thiol groups and glutathione [33]. Our results confirm that UVA irradiation induces an oxidative stress in the cornea, which correlates with macromolecular alterations. However, the different corneal layers exhibit different sensitivity and responsiveness to UVA. This suggests that UVA-induced oxidative events in the cornea strongly depend on cells type and microenvironment. Moreover, taken together, our results shed light on a greater susceptibility of the endothelium to UVA-induced oxidation-related toxicity.

2. Materials and methods

All experiments performed in this study were conducted in accordance with our institution's guidelines, the Declaration of Helsinki and the ARVO Animal Statement. Research protocols using human corneal cells received approval by the *Centre de Recherche du CHU de Québec* (CRCHUQ) institutional committee for the protection of human subjects.

2.1. UVA irradiation

Rabbit heads from young non-albinos rabbits were obtained from a local slaughterhouse. The rabbits were not genetically chosen. Eyes were enucleated upon reception of heads. Four pairs of rabbit eyes were used to assess the consequences of UVA exposure in the cornea. For each pair, one eye was irradiated *ex vivo* on ice with 600 J/cm^2 UVA (“UVA”), while the other was left unirradiated on ice (“No UV”) to serve as a control. Irradiation was achieved using B100 lamps (UVP Upland, CA) with an emission peak at 365 nm (Fig. 2). The emission spectrum of the UVA lamps consists of > 99.99% of UVA-I wavelengths (340–400 nm) and contains no significant UVB wavelengths. Irradiance on the surface of the eyes ranged from 15.4 to 19.3 mW/cm^2. As a result, irradiation lasted between 8.6 and 10.8 h. During the irradiation, controls and UVA-irradiated eyes were regularly moistened with cold phosphate buffer saline (PBS) to prevent heating and drying out of the

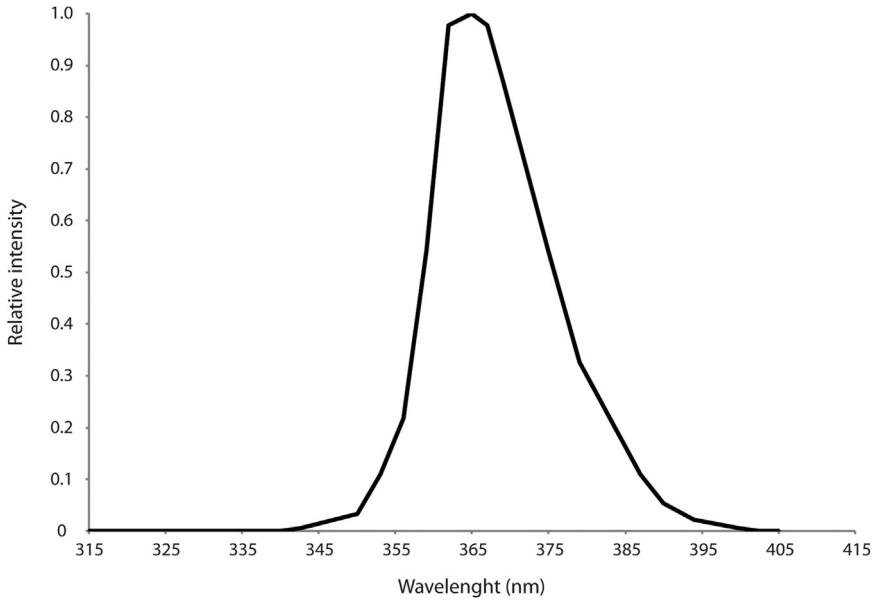

Fig. 2. Emission spectrum of the UVA lamps. UVA irradiation was achieved using B100 Series 365 nm lamps with filter (UVP, Upland). The spectrum is derived from manufacturer's specifications and modified according to measurements made using an International Light double monochromator spectroradiometer (IL7000/760D/790).

cornea.

2.2. Cornea preparation

At the end of irradiation, control and UVA-irradiated eyes were immediately dissected to isolate the cornea from the rest of the eye. Three additional eyes from 3 different rabbit heads were also dissected and their corneas collected without delay after enucleation. These eyes did not undergo any procedure. Isolated corneas were then embedded in water based Tissue-Tek® O.C.T compound (Sakura Finetek) and kept at −80 °C until further use. For fluorescence analysis, 5 µm thick slices were obtained from cryopreserved tissues using a Leica MC3050 cryostat, and heat-fixed on a microscope slide. For quantitative real-time PCR (qPCR) analysis, 150 µm thick slices were trimmed and laid on a microscope slide. The epithelium and the anterior half of the stroma was mechanically separated from the rest of the cornea under a dissecting microscope, and used for DNA extraction. DNA was extracted with the DNeasy Blood and Tissue Kit (Qiagen) according to the manufacturer's protocol, with an RNase treatment.

2.3. Redox status analysis

Corneal oxidation-reduction states have been monitored by analyzing the fluorescent emissions of two cellular fluorophores: the oxidized form of mitochondrial flavins ($^{ox}Fv_m$) and the reduced form of pyridine nucleotides NAD and NADP (NAD(P)H). Mitochondrial flavins and pyridine nucleotides are important and abundant soluble metabolic coenzymes, with significant redox-dependent responses [34,35]. $^{ox}Fv_m$ and NAD(P)H forms are naturally fluorescent, and display well separated excitation and emission spectra. $^{ox}Fv_m$ have a broad excitation and emission spectra with peaks at ~460 and 540 nm, respectively, while NAD(P)H excitation and emission spectra peak at ~366 and 440 nm, respectively. Moreover, signals from both forms correlate with their distribution and concentration. The ratio of the two fluorescence intensities is a reliable indication of intracellular redox states in tissues [34,36]. Based on the respective excitation and emission spectra of $^{ox}Fv_m$ and NAD(P)H, images of $^{ox}Fv_m$ and NAD(P)H fluorescence in 5 µm corneal slices were then sequentially captured, using a Zeiss Axioimager Z2 microscope equipped with appropriate filter sets and coupled with a Zeiss AxioCam MRm Rev 3 Monochromatic Digital Camera. Alongside this, mitochondria in the 5 µm corneal slices labelled with 100 nM of chloromethyl-X-rosamine (CMXRos; Mito-Tracker Red – Invitrogen) for 15 min at room temperature, were also imaged.

For analysis, each cornea was defined in 3 measurement areas (epithelium, stroma and endothelium). Epithelia and stroma were then subdivided in 3 and 10 strata, respectively, to obtain a measure of fluorescence intensities as a function of depth within the cornea. This also enables to normalize for corneal depth differences between specimens. Quantification of fluorescent signals from $^{ox}Fv_m$, NAD(P)H and mitochondria was done in each stratum using the "AutoMeasure" module of Zeiss Axiovision Imaging System. After correcting for camera background intensities, a redox ratio of $^{ox}Fv_m$ signal divided by NAD(P)H signal was computed for each stratum. The analysis was carried out on at least four separated regions on each rabbit cornea, and an average $^{ox}Fv_m$/NAD(P)H signals ratio was determined for every stratum in each cornea. The statistical two-tailed paired Student *t*-test was applied to assess differences between "No UV" and "UVA" conditions. Significance level was defined for p-value ≤ 0.05.

2.4. Immunofluorescence

For 8-OHdG staining, 5 µm corneal slices were fixed with cold methanol, 10 min at −20 °C. Samples were then treated with 5 mg/mL RNase A, permeabilized with 0.1% Tween® 20 (Fisher Bioreagents), and DNA was denatured using 2 N HCl solution for 10 min. Samples were incubated overnight at 4 °C with a mouse anti-8 Hydroxyguanosine monoclonal antibody [N45:1] (Abcam) diluted 1:100, and then incubated 1 h at 37 °C with a goat anti-mouse IgG (H + L) polyclonal antibody conjugated to Alexa Fluor 647 (Jackson ImmunoReseach) diluted 1:2500. Mitochondria or nuclear DNA were counterstained at room temperature using 100 nM of MitoTracker Red CMXRos (Invitrogen) for 15 min or 0.33 µg/mL propidium iodide (PI – Invitrogen) for 10 min, respectively. For PSSG staining, sections were fixed in 4% formaldehyde for 10 min at room temperature, treated with 5 mg/mL RNase A and permeabilized with 0.15% Triton X-100. Treated samples were incubated overnight at 4 °C with mouse monoclonal anti-glutathione antibody [clone D8] (Abcam) diluted 1:100, and then incubated with a goat anti-mouse IgG (H + L) polyclonal antibody conjugated to Alexa Fluor 647 (Jackson ImmunoReseach) diluted 1:2500, for 1 h at room temperature. Nuclear DNA was counterstained with 20 µg/mL of PI for 10 min at room temperature. Slides were

mounted with Slowfade Gold antifade reagent (Invitrogen). Using CMXRos or PI as a reference dye, we quantified fluorescent signals from 8-OHdG in mitochondria or nuclear DNA throughout the entire corneas, as described above. For mitochondrial 8-OHdG, after correcting for camera background intensities, "8-OHdG signal/mitochondria signal" ratios were derived in order to minimize distribution bias caused by variations of mitochondrial density across cellular layers. For nuclear DNA, after correction, mean 8-OHdG fluorescence intensities of all nuclei were averaged in each stratum. Analysis was performed as described above. For PSSG analysis, corneas were defined in 3 measurement areas (epithelium, stroma and endothelium) and the stroma was subdivided in 3 areas. Quantification was done as described above. Corrected PSSG signals were then divided by the number of nuclei to derive the mean "PSSG fluorescence intensity/cell" for each area. Analysis was performed as described above.

2.5. Quantitative real-time PCR (qPCR)

Mitochondrial DNA (mtDNA) copy number was quantitatively estimated by qPCR on a Rotor-Gene Q real-time thermocycler (Qiagen). Relative levels of mtDNA were determined using primers sets designed to amplify total mtDNA [37]. These primers are specific for the 7S DNA coding region (5′ – AAT CAA TTG GCG ACC AAT GG and 5′ – CGC CTG GTT CTA GGA ATA ATG G). MtDNA amplification was achieved using 30 ng of total DNA. For each sample, a standard curve (with 5, 1, 0.2, 0.05, 0.005 and 0.001 ng total DNA/reaction) was also generated using 18 S nuclear DNA coding region specific primers (5′ – TAG AGG GAC AAG TGG CGT TC and 5′ – CGC TGA GCC AGT CAG TGT) [38]. The amplification level of mtDNA primers was then compared with the standard curve and a relative level of mtDNA was inferred.

PCR reactions were performed in 1X Brilliant III Ultra-Fast SYBR® Green qPCR Master Mix (Agilent Technologies) and 0.5 µM of each primer. For each sample, mtDNA amplification was realized in quadruplicate. A negative control (no DNA) was included in each run. PCR cycles were as follow: 95 °C incubation during 3 min followed by 40 cycles of denaturation at 95 °C for 20 s and annealing/extension at 60 °C for 20 s. Amplification levels and standard curves were generated using the Rotor-Gene Q analysis software. The non-parametric statistical Wilcoxon signed-rank test was applied to assess differences in relative mitochondrial DNA density between No UV and UVA samples.

3. Results

3.1. The posterior half of the cornea is more prone to UVA-induced oxidative stress

The cornea absorbs photons in the 340–400 nm UVA-I range (Fig. S1). Removal of the endothelium induces no significant variation (less than 3%) of UVA-I overall corneal transmittance, showing that epithelial and stromal layers are the main contributors to corneal absorbance in those wavelengths. Measure of transmittance after de-epithelialization of the stroma reveals that the epithelium absorbs around 15% of UVA-I (Fig. S1). To evaluate the extent of cellular oxidative stress induced upon UVA radiations absorption by corneal layers, corneal redox state has been determined in 4 pairs of UVA-exposed (600 J/cm^2) and unirradiated rabbit eyes. This was achieved using "oxidized mitochondrial flavins"/"reduced pyridine nucleotide" ($^{ox}Fv_m$/NAD(P)H) signal ratio measurements. The effect of UVA irradiation on $^{ox}Fv_m$ and NAD(P)H fluorescent emissions within entire rabbit corneas is shown in Fig. 3A–C. Fig. 3D illustrates the resulting UVA-induced changes in corneal redox state as a function of corneal depth.

In response to UVA irradiation, signal from $^{ox}Fv_m$, the oxidized species indicator, significantly increases throughout the cornea (Fig. 3A and B). This increase is more pronounced in the epithelium than in any other corneal layers, which is consistent with UVA wavelength penetrance. More precisely, $^{ox}Fv_m$ signals is in average 4.5 (± 1.4) times stronger in epithelia from UVA-exposed corneas than in control epithelia. In stromal and endothelial layers, UVA irradiation induces 1.8 (± 0.4) time and 1.7 (± 0.2) time higher $^{ox}Fv_m$ signal intensities, respectively (Fig. 3B). Fluorescence signals from the reduced species indicator, NAD(P)H, also rise in response to UVA, but not in the entire cornea. Once again, the more important UVA-induced variations are observed in epithelia, with a 3.3 (± 0.9) times averaged increase in NAD(P)H signal intensity (Fig. 3A and C). In stroma, NAD(P)H fluorescence intensities are 1.3 (± 0.2) time higher after UVA exposure. In the endothelial layer however, NAD(P)H fluorescence remains unchanged by UVA exposure (Fig. 3C).

Since $^{ox}Fv_m$ signals increase more than NAD(P)H signals along the whole UVA-exposed corneas, the redox potential, expressed as $^{ox}Fv_m$/NAD(P)H signal ratio, is increased (Fig. 3D). This indicates that UVA exposure leads to an oxidized state in corneal cells. However, the $^{ox}Fv_m$/NAD(P)H signal ratio changes induced by UVA irradiation is significant ($p < 0.05$) only in the posterior part of the cornea (middle stroma to endothelium). UVA-induced variation in $^{ox}Fv_m$/NAD(P)H signal ratio seems to increase with increasing corneal depth. In the middle portion of the stroma, $^{ox}Fv_m$/NAD(P)H ratio is increased by 39% following UVA treatment. In the posterior stroma and in the endothelium, UVA irradiation leads to an increase by 46% and 61% of the redox ratio values, respectively. Taken together, our data confirm that UVA exposure initiates redox imbalance and therefore can promote oxidative stress in the cornea. Unexpectedly, UVA rays induce a greater oxidation in the posterior side of the cornea, with the corneal endothelium being the most affected layer.

3.2. UVA induce mitochondrial transmembrane potential disruption on corneal anterior side

$^{Ox}Fv_m$ and NAD(P)H fluorescence signals mostly originate from mitochondrial matrix space [34]. We thus directly assessed mitochondria state in UVA-exposed and unirradiated corneas (Fig. 3A), using a CMXRos (MitoTracker Red) dye. CMXRos dye is a cationic selective fluorescent probe, relying on mitochondrial transmembrane potential to accumulate in mitochondria. Analysis of CMXRos fluorescence levels reveals a significantly higher CMXRos fluorescence in the anterior side of UVA-irradiated corneas when compared to control corneas anterior side (Figs. 3A and 4A). More precisely, in the epithelium strata and in the anterior third of the stroma, we measured a 1.9 (± 0.8) time and 1.3 (± 0.2) time UVA-induced increase in CMXRos fluorescence, respectively. No significant variation in the dye fluorescence was observed in the rest of the cornea.

To rule out the possibility that the observed UVA-induced changes in CMXRos fluorescence intensity were due to UVA-related variations in mitochondrial mass, we compared by qPCR the mitochondrial DNA (mtDNA) copy number in the anterior portion of each corneal pair. We found no differences in mtDNA copy number between UVA-exposed and unirradiated samples (Fig. 4B), indicating similar amounts of mitochondria between the two corneas of each pair. Therefore, the observed increase in CMXRos staining intensity most likely reflects changes in the mitochondrial polarization status and/or in mitochondrial morphology.

3.3. UVA induce different oxidative DNA damage accumulation patterns in nuclei and mitochondria

We assessed the extent and distribution of UVA-induced cellular component oxidation in different corneal layers. We first investigated UVA-induced oxidative DNA damage throughout the cornea using 8-OHdG as an indicator of DNA oxidation. This was achieved by quantitative fluorescent immunolabeling of 8-OHdG. The ability of our assay to reliably detect and quantify oxidative DNA damage was validated (Supplementary methods and Figs. S2–S4). Quantitative

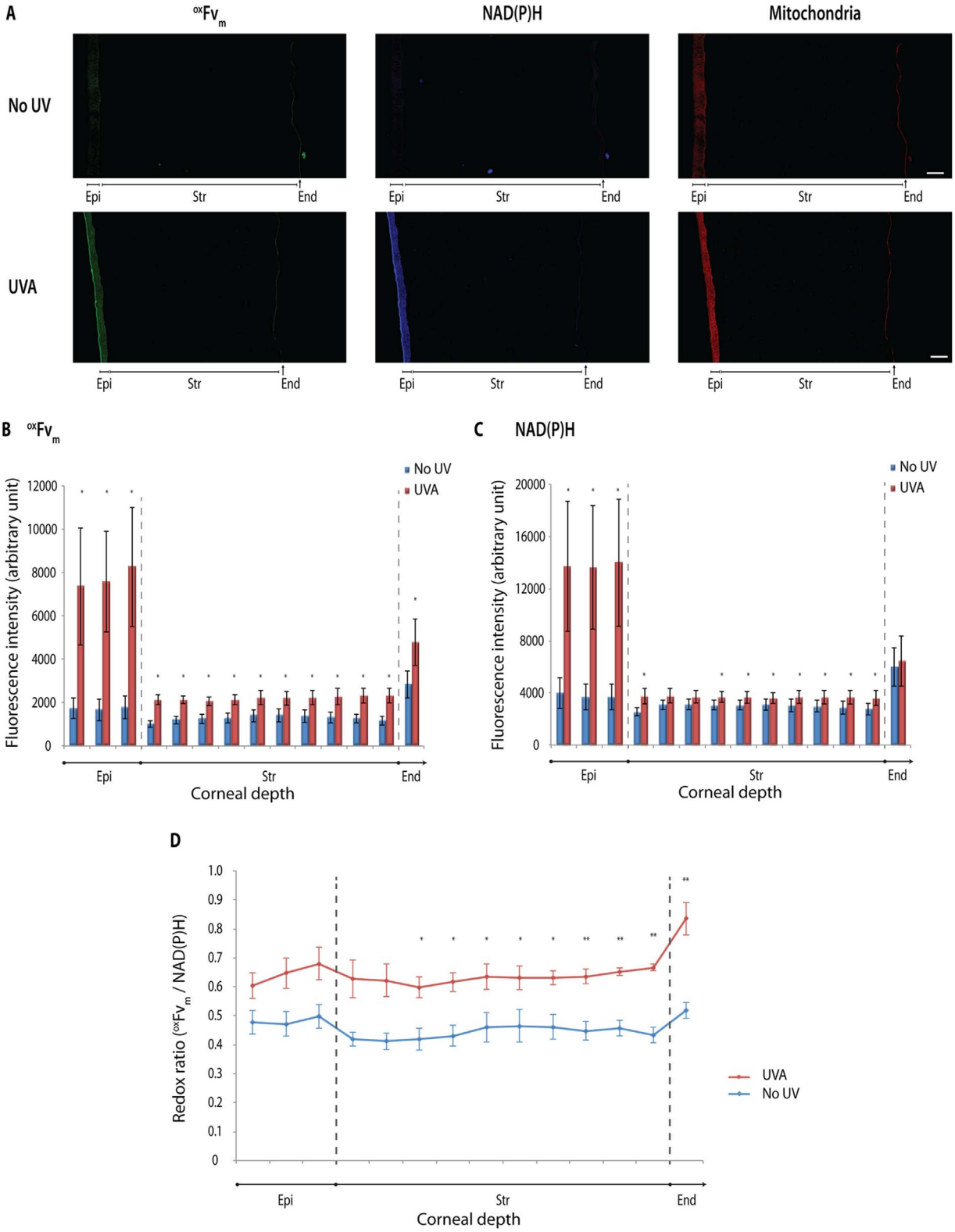

Fig. 3. Corneal redox states response to UVA exposure. Rabbit eyes were irradiated *ex vivo* with 600 J/cm^2 of UVA. (A) Representative $^{ox}Fv_m$ (green) and NAD(P)H (blue) intrinsic fluorescence imaging in unirradiated (No UV) and irradiated (UVA) corneas. Mitochondria (red) were labelled with MitoTracker Red (scale bar = 50 μm). (B) Quantification of $^{ox}Fv_m$ intrinsic fluorescence signals in corneal epithelium, stroma and endothelium from unirradiated (No UV) and UVA-irradiated (UVA) corneas. (C) Quantification of NAD(P)H intrinsic fluorescence signals in corneal epithelium, stroma and endothelium from unirradiated (No UV) and UVA-irradiated (UVA) corneas. (D) Effect of UVA exposure on the redox ratio. In each stratum, a $^{ox}Fv_m$/NAD(P)H signal ratio was calculated to derive the redox ratio. Experiments were performed using 4 pairs of rabbit eyes. For each cornea, measures have been carried out on at least 4 separated regions and then pooled together. Error bars are standard error of the mean (SEM). Differences between "No UV" and "UVA" conditions were assessed using the two-tailed paired Student *t*-test (*$p < 0.05$; **$p < 0.01$). Epi: epithelium; Str: stroma; End: endothelium. (For interpretation of the references to color in this figure legend, the reader is referred to the web version of this article).

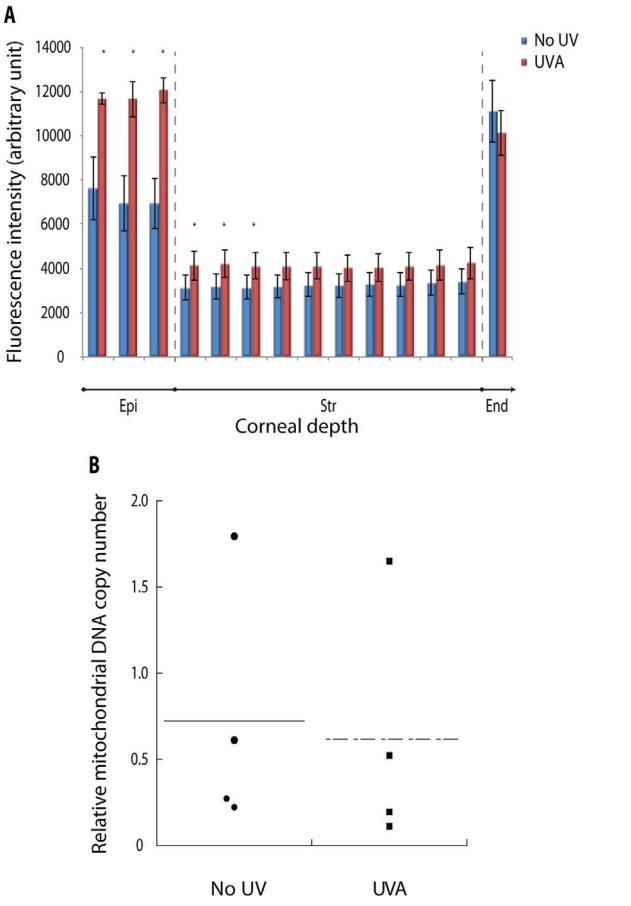

Fig. 4. Effect of UVA exposure on mitochondrial membrane potential and mitochondrial DNA copy number. Rabbit eyes were irradiated *ex vivo* with 600 J/cm^2 of UVA. (A) Mitochondria in unirradiated (No UV) and irradiated (UVA) rabbit corneas were labelled with MitoTracker red CMXRos, and CMXRos signal was quantified along corneal epithelium, stroma and endothelium. Experiments were performed using 4 pairs of rabbit eyes. For each cornea, measures have been carried out on at least 4 separated regions and pooled together. Error bars are SEM. Differences between "No UV" and "UVA" conditions were assessed using the two-tailed paired Student *t*-test (*$p < 0.05$). (B) Total DNA, including mitochondrial DNA (mtDNA), was extracted from the anterior part (epithelium and anterior stroma) of the 4 pairs of unirradiated and UVA-irradiated rabbit corneas. mtDNA density per cell has been assessed by Q-PCR using a ratio of the mtDNA level over a known copy number per cell gene (the nuclear encoded 18 S ribosomic subunit). The non-parametric Wilcoxon signed-rank test was applied to assess differences in relative mtDNA density between "No UV" and "UVA" samples. Epi: epithelium; Str: stroma; End: endothelium. (For interpretation of the references to color in this figure legend, the reader is referred to the web version of this article).

fluorescent immunolabeling of 8-OHdG in UVA-exposed and unexposed corneas revealed that UVA-induced DNA damage colocalize with mitochondria (Fig. 5A and Fig. S5B) and with nuclear DNA (Fig. 5B and Fig. S5C). Surprisingly, 8-OHdG/mitochondria signal analysis indicates that significantly less mitochondrial 8-OHdG is present in corneal epithelial cells of UV-exposed eyes (Fig. 5C), when compared to related unirradiated eyes kept on ice for the duration of irradiation (blue trace) or to unirradiated eyes analyzed immediately after enucleation (dashed line). More precisely, relative levels of epithelial mitochondrial 8-OHdG are in average 0.25 for UV-exposed corneas, 0.49 and 0.50 for related unirradiated and baseline samples, respectively (Fig. 5C). In the corneal stroma and endothelium, UVA exposure is associated with higher mitochondrial 8-OHdG levels, although not statistically significant.

In nuclei, 8-OHdG are generally more frequent in UVA-exposed corneas than in unexposed corneas (Fig. 5D). Specifically, UVA-induced 8-OHdG accumulation in nuclei was significant in all stromal strata. We found an average of 1.8 (± 0.3) times higher 8-OHdG level in nuclei of stromal cells. Conversely, the epithelium, the most UV-exposed part of the cornea, shows little or no UVA-induced 8-OHdG accumulation on its outermost stratum (Fig. 5B, D and Fig. S5C). Uneven UV-induced 8-OHdG accumulation occurs in the middle and basal epithelial strata, with some nuclei being strongly damaged while quite a few show little or no lesions (Fig. 5B). Consequently, UV-dependent 8-OHdG induction in the entire epithelial strata is not statistically significant. In the endothelium, there is an increase in UVA-induced nuclear 8-OHdG, but it did not reach significance level ($p = 0.07$). Collectively, the data show that mitochondrial and nuclear DNA have different susceptibilities to UVA-induced DNA oxidation, in the native configuration of the cornea.

3.4. UVA induce transient protein oxidation in epithelial and endothelial corneal layers

We investigated UVA-induced alterations of redox-active proteins, using the level of S-glutathionylated proteins (PSSG). Fluorescent immunolabeling of PSSG shows that UVA exposure leads to the S-glutathionylation of cytosolic proteins far more than those in the nucleus (Fig. 6A). However, compared to the other parameters investigated, we found that UVA rays induce variable S-glutathionylation patterns from rabbit to rabbit.

As illustrated in Fig. 6B, PSSG analysis in UV-exposed and unirradiated corneas reveals a significant increase in oxidized protein levels in the epithelial and endothelial corneal layers ($p < 0.05$) associated with UVA exposure. Indeed, compared to unirradiated controls levels, PSSG are 2.4 (± 1.2) and 1.4 (± 0.2) times more frequent in UVA-exposed corneal epithelia and endothelia, respectively. No significant levels of PSSG were measured in the stroma of UV-exposed or unirradiated corneas (Fig. 6B). Taken together, the results shed some light on the transient UVA-induced alterations of redox-active proteins in the cytosol of corneal epithelial and endothelial cells.

4. Discussion

A single exposure of 600 J/cm^2 broadband UVA-I light (340–400 nm with a pic at 365 nm) was used to irradiate the rabbit eyes (Fig. 2). Kurtin and Zuclich [39] reported that, for oxygen-dependent photochemical damage mechanisms to occur in corneal tissue, the threshold exposure dose varies from 58 to 258 J/cm^2 with monochromatic wavelengths ranging from 340 to 400 nm [39]. In our study, a wavelength-summed effective dose of 600 J/cm^2 was chosen to ensure that the major spectral components of our lamp source were delivered to a dose sufficient enough to cause damage.

Following irradiation, we have analyzed UVA immediate effects on cellular redox state and on mitochondrial membrane potential in rabbit corneas *in situ*. Immunofluorescence labeling enabled us to localize and estimate the amount of 8-OHdG, the major UVA-induced oxidative DNA lesion. Together, these parameters provide an indication of the susceptibility of each corneal layer to UVA-generated harmful alterations. Using the level of PSSG, we have analyzed UVA-induced changes in oxidatively altered redox-active proteins patterns. Free thiol groups of proteins cysteinyl residues are readily and reversibly modified by glutathione under oxidative stress conditions (reviewed in [40] and [41]), such as the one induced by UVA irradiation [42]. Glutathione is ubiquitously expressed as reduced (GSH) and oxidized (GSSG) glutathione but it is preferentially maintained in its reduced form in mammalians cells [43] and represents the most abundant low-molecular-weight reducing agent. Given that glutathionylated cysteine residues are generally resistant to further irreversible oxidation, proteins S-glutathionylation has been suggested to be an adaptive defense against oxidative insults, protecting critical regulatory proteins from permanent damage [41,44]. This process has also been proposed as a mean to prevent glutathione efflux from cell under oxidative stress condition [33,40] and to be an important regulatory mechanism of signal transduction pathways activated in response to stress [41,45]. In

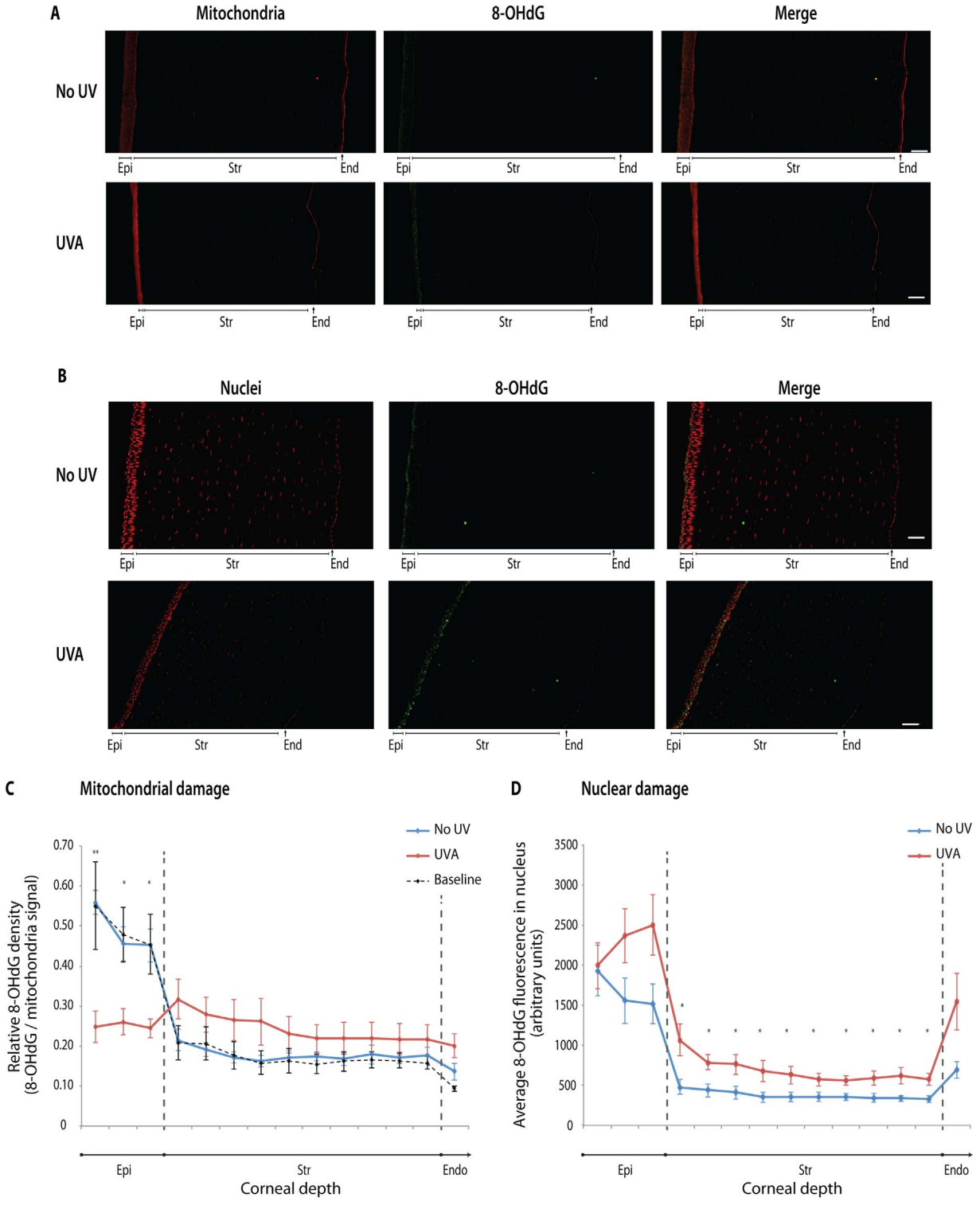

Fig. 5. UVA-induced DNA oxidation along the cornea. Rabbit eyes were irradiated *ex vivo* with 600 J/cm^2 of UVA. 8-OHdG were measured along unirradiated (No UV) and irradiated (UVA) corneas by fluorescent anti-8OHdG immunostaining. (A) Representative 8-OHdG (green) staining along corneal epithelium, stroma and endothelium of unirradiated (No UV) and irradiated (UVA) corneas. Mitochondria (red) were counterstained with MitoTracker Red (scale bar = 50 μm). (B) Representative 8-OHdG (green) staining along corneal epithelium, stroma and endothelium of unirradiated (No UV) and irradiated (UVA) corneas. Nuclear DNA (red) was counterstained with propidium iodide (scale bar = 50 μm). (C) Quantification of fluorescence intensity of 8-OHdG signals colocalizing with mitochondrial signal along "No UV" and "UVA" corneal epithelium, stroma and endothelium. Intensity of 8-OHdG signals colocalizing with mitochondrial signal along corneas from 3 eyes analyzed immediately after enucleation were also measured ("baseline"). "8-OHdG signal/mitochondria signal" ratios were derived in order to minimize distribution bias caused by variation of mitochondrial density across cellular layers. (D) Quantification of fluorescence intensity of 8-OHdG signals colocalizing with nuclear DNA signal along "No UV" and "UVA" corneal epithelium, stroma and endothelium. Experiments were performed using 4 pairs of rabbit eyes. Each cornea was tested on at least 4 separated regions. Error bars are SEM. Differences between "No UV" and "UVA" conditions were assessed using the two-tailed paired Student *t*-test (*$p < 0.05$; **$p < 0.01$). Epi: epithelium; Str: stroma; End: endothelium.

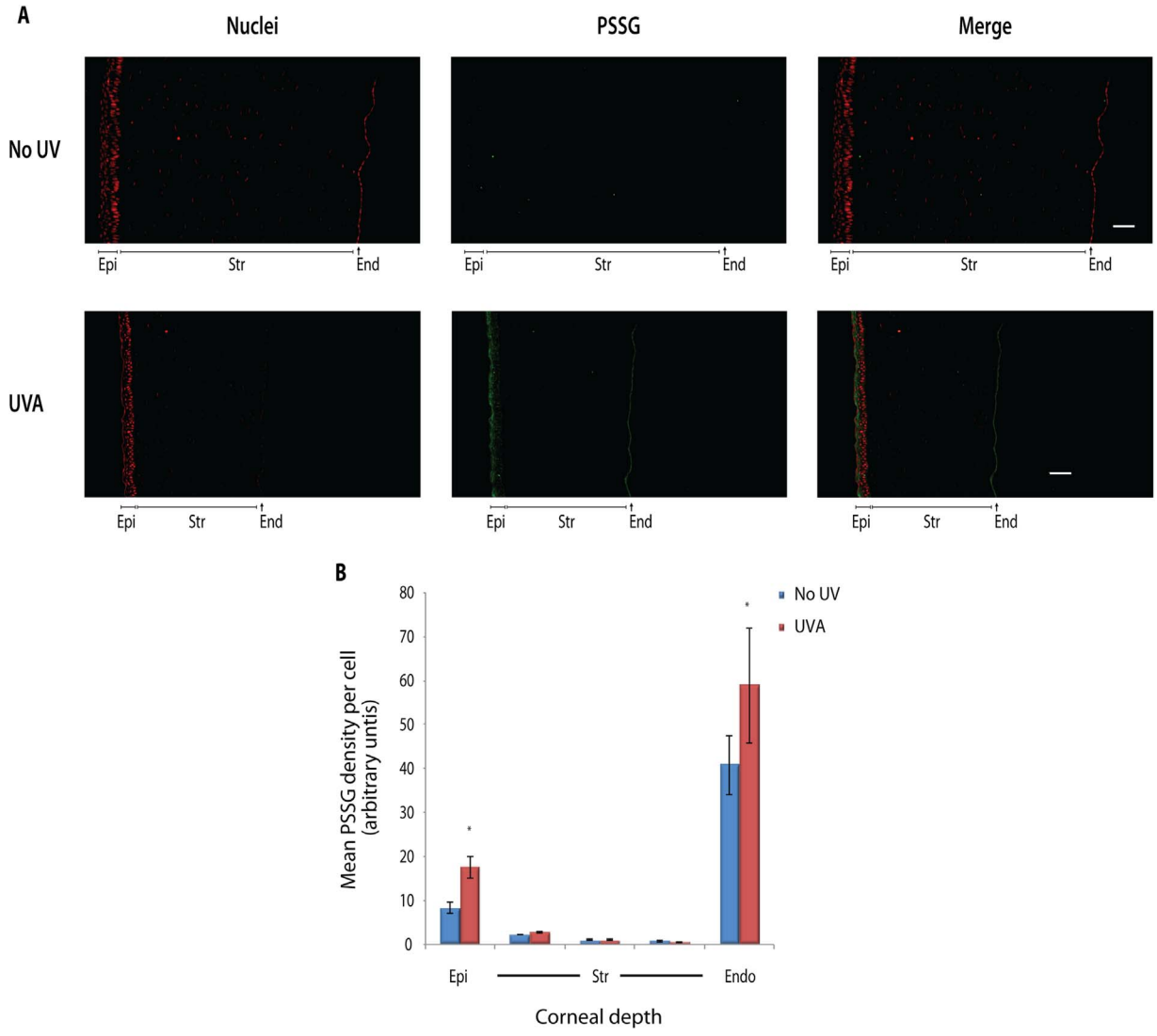

Fig. 6. UVA-induced S-glutathionylation of proteins along the cornea. Rabbit eyes were irradiated *ex vivo* with 600 J/cm^2 of UVA. UVA-induced PSSG were measured along unirradiated (No UV) and irradiated (UVA) corneas by fluorescent anti-PSSG immunostaining. (A) PSSG (green) staining along corneal epithelium, stroma and endothelium of unirradiated (No UV) and irradiated (UVA) corneas. Nuclear DNA (red) was counterstained with propidium iodide (scale bar = 50 μm). (B) Quantification of PSSG fluorescence signals along corneal epithelium, stroma and endothelium of unirradiated (No UV) and UVA irradiated (UVA) corneas. In each layer, total fluorescence intensity was divided by the number of nuclei to derive a mean fluorescence signal per cell. Experiments were performed using 4 pairs of rabbit eyes. Each cornea was tested on at least 4 separated regions. Error bars are SEM. Differences between "No UV" and "UVA" conditions were assessed using the one-tailed paired *t*-test (*$p < 0.05$). Epi: epithelium; Str: stroma; End: endothelium. (For interpretation of the references to color in this figure legend, the reader is referred to the web version of this article).

this study, PSSG levels were thus assessed to provide an indication of corneal layers redox sensing capacity and ability to cope with UVA toxicity.

4.1. The corneal epithelium efficiently deals with UVA-induced early oxidation

Corneal layers absorbance properties play an important role in determining their sensitivity to exposure. The corneal epithelium has a higher absorption coefficient than the rest of the cornea in all UV spectra [46]. Thus, as confirmed by our data (Fig. S1), the corneal epithelium absorbs relatively high amounts of UVA photons. However, despite an oxidative shift in its redox state, the epithelium has the less compromised mitochondrial redox balance after UVA exposure (Fig. 3D). UVA irradiation induces a significant oxidation within the epithelium (4.5 times average increase in $^{ox}FV_m$ signals) but this increase is compensated by a 3.3 times average increase in mitochondrial reducing equivalents indicators, NAD(P)H (Fig. 3). NADH and NADPH share similar fluorescence properties but have distinct functions in cells (reviewed in [47]). NADPH pools are necessary to maintain GSH/GSSG ratio in levels required for cells viability and functions. A major source of NADPH is the pentose phosphate pathway (PPP) [47]. It has been reported that the activity of the glucose-6-phosphate dehydrogenase, the rate-limiting enzyme of the PPP, was significantly enhanced (up to 69%) in porcine corneas after a 6 h exposure to UVA [31]. The authors suggested that UVA exposure of corneas stimulates the PPP, increasing the level of NADPH and thus strengthening antioxidative corneal defenses. A similar stimulation of NADPH generation may partly account for the UVA-related increase in NAD(P)H levels observed in our model. It is noteworthy that, while mitochondrial NAD(P)H exist mainly as free compounds, more than 80% of NAD(P)H fluorescence arise from enzyme-bound NAD(P)H [48,49]. Observed increases in NAD(P)H signals may then also be partly explained by a higher relative proportion of enzyme-bound NAD(P)H, resulting from an enhanced consumption of free NAD(P)H by NAD(P)H-dependent enzymes [35,49] in response to UVA exposure. This would reflect a UVA-induced stimulation of specific enzymatic activities within the epithelium.

Preferential accumulation of corneal GSH and high GSH/GSSG ratios have been described in the epithelium [50], giving this corneal layer a high sensitivity to perturbations in redox status and would lead to a rapid initial response potential. Indeed, in our experiments, epithelia showed the most UVA-related increase in modified redox-active proteins (Fig. 6). Epithelial cells are thus expected to modulate redox-dependent proteins (including transcription factors, mitochondrial complex I enzymes, chaperones and antioxidant enzymes [25,51]) early after UVA exposure to rapidly transduce redox status perturbations into a functional response.

In agreement with an early adaptive response to UVA, nuclear and mitochondrial early accumulation of UVA-induced 8-OHdG seems effectively prevented or reduced in epithelial cells (Fig. 5C and D). Similar mitochondrial levels of 8-OHdG were measured in unirradiated eyes kept on ice for the duration of irradiation and in unirradiated eyes analyzed immediately after enucleation. This indicates that our experimental setting do not alter 8-OHdG relative formation/removal along the cornea. Surprisingly, in UVA-exposed corneal epithelia, 8-OHdG level was significantly lower (2-fold) than in both unirradiated groups, suggesting that in UVA-exposed corneal epithelia, lesion removal occurs faster than formation. This might suggest that mitochondrial DNA repair systems are enhanced in the epithelium in response to UVA exposure.

Despite the aforementioned evidences of corneal epithelial cells capacity to cope with UVA-induced oxidation, mitochondria in epithelia seem strongly affected by UVA. Indeed UVA irradiation leads to changes in the staining pattern of mitochondria, along with unchanged amount of mitochondrial DNA. This suggests that UVA exposure has modified the structural and possibly functional features of mitochondria. In view of the marked UVA-induced accumulation of NAD(P)H in epithelial cells, potential alterations in the electron transport chain and mitochondrial dysfunctions might have occurred. We suggest that these staining pattern changes reflect the first steps of an opening of the mitochondrial permeability transition pore (PTP). PTP opening results in an increased influx of cations and water in mitochondria, leading to a rapid loss of mitochondrial membrane potential and release of mitochondrial apoptotic factors [26].

Taken together, our data indicate that the epithelium is strongly affected by UVA exposure. This is evidenced by substantial UVA-induced increases in $^{ox}Fv_m$, NAD(P)H, PSSG epithelial levels. However, while being the most UVA-exposed part of the cornea, the epithelium is able to limit the extent of cellular damage caused by UVA. Epithelial cells reducing capacities partly compensate for UVA-induced oxidation and seem able to prevent 8-OHdG accumulation in their DNA. Their response could provide an additional protection from UVA for the underlying layers.

4.2. Low early adaptive potential to UVA-induced oxidation in the corneal stroma

Due to its thickness, UVA absorbance of whole stroma is higher than that of the others layers [46,52]. As a whole, it is responsible for more than two-third of corneal total UVA absorbance (Fig. S1), and no difference in UV absorbance characteristics is observed between layers from anterior, middle and posterior stroma [46]. In our model, UVA-induced redox balance disruption in the stroma seems inversely related to UVA penetrance. Compared to the epithelium, UVA-induced $^{ox}FV_m$ signal increase is significantly reduced, confirming that the epithelium acts as an effective UVA filter (Fig. 3B). We found no significant UVA-associated changes in the redox status of the stromal part underlying the epithelium (Fig. 3D). However, UVA-induced variations in mitochondrial staining patterns in this portion were observed, although to a lesser extent than in the epithelium (Fig. 4A). This suggests that cells in the anterior portion of the stroma may also experience a UVA-induced mitochondrial PTP disruption. In the middle and posterior portions of the stroma, $^{ox}Fv_m$/NAD(P)H ratios following UVA exposure were increased but PSSG were barely detectable throughout the stroma (Fig. 6). Those markers indicate that early adaptation to UVA-induced oxidation is rather low in the stroma. This is consistent with the quiescent state of keratocytes in native corneal stroma and suggests that stromal response to UVA relies on delayed mechanisms. The absence of a PSSG-mediated early adaptation of stromal cells to UVA is supported by UVA-induced significant accumulation of 8-OHdG in keratocytes nuclei, as well as by the higher (although not statistically significant) level of mitochondrial 8-OHdG in exposed corneal stroma (Fig. 5).

Since proteins are the major target of ROS, PSSG low levels in irradiated stroma also suggest that proteins in stromal cells are highly susceptible to UVA-induced irreversible oxidation. As a result, under prolonged or chronic exposure to UVA, keratocytes in the stroma should be more sensitive to oxidative damage accumulation. This is in agreement with previous reports showing that age-related mitochondrial DNA mutations in the cornea, probably catalyzed by UVA light, were concentrated in the stroma [37,53]. But given that keratocytes in the anterior part are more resistant to UVA-induced redox balance disruption and display mitochondrial structure effects similar to that of epithelial cells, there might be a communication between epithelium and stroma that may regulate keratocytes sensitivity and responsiveness to UVA toxicity in the anterior part of the stroma.

4.3. Potential altered functions of the corneal endothelium

By the UVA filtering action of the epithelium and the stroma, the endothelium is the corneal layer the less heavily exposed to UVA. But with a redox ratio increased by 61% after UVA exposure, the endothelium is the corneal layer the most susceptible to UVA-induced early pro-oxidant state. Unlike the epithelium, no NAD(P)H increase occurs to compensate for UVA-related $^{ox}Fv_m$ increase in the endothelial cells (Fig. 3). The corneal endothelium is responsible for maintaining stroma in a relative dehydration state required for corneal transparency [54], a function highly dependent on glutathione [55,56]. It is one of the highest metabolically active layers in the eye [57]. Corneal endothelial cells are therefore rich in mitochondria and are exposed to high basal ROS levels. As a consequence, an additional load of ROS from an exogenous source, like UVA irradiation, can easily induce a condition of oxidative stress in endothelial cells.

Despite the marked redox imbalance induced by UVA in the endothelium, UVA-generated 8-OHdG accumulation in nuclei and mitochondria of corneal endothelial cells was not significant (Fig. 5). To counteract oxidative stress, healthy endothelial corneal cells normally express ubiquitous antioxidants such as catalase and glutathione peroxidases/transferases [58], along with an important defense system of antioxidant enzymes, under the control of the nuclear factor erythroid-2 related factor-2 (Nrf2) [28,59]. Metallothioneins, cytoglobins superoxide dismutases, peroxiredoxins and thioredoxin reductases are part of this defensive system. Nrf2-dependent antioxidant system may contribute to prevent the formation of 8-OHdG under oxidative stress. It has been reported that corneal endothelial cells showing depleted levels of Nrf2 have significantly more oxidative DNA lesions than normal cells [59].

We measured the highest basal level of PSSG per cells in the endothelium (Fig. 6). This may result from the high metabolic activity of this layer, yielding important physiological amount of ROS. Endothelial PSSG levels were significantly increased by UVA exposure, suggesting that adaptive response of the endothelium to UVA can be promptly triggered. However S-glutathionylation would induce a loss of free glutathione required for endothelial pump and barrier functions [56]. A decrease of endothelial intracellular glutathione below one-third of its normal level has been found to severely impair endothelial function and results in abnormal corneal hydration [56]. Rapid NADPH-dependent turnover and/or uptake of GSH from aqueous is then required under oxidative stress to maintain endothelial cells function [56,58]. We detect no early compensatory increase of en-

dothelial NAD(P)H in our model, but turnover of GSH cannot be ruled out. Uptake of GSH from aqueous might be implicated in the early phase of endothelial adaption to UVA-induced oxidation to prevent endothelial function collapse.

Taken together, our data show that, in their native conformation, the different corneal layers display different sensitivity and reactivity potential to UVA-induced stress. Owing to its absorbance properties, the corneal epithelium is subjected to important alterations in response to UVA-induced oxidation. However, it displays a prompt responsiveness to UVA and can, to some extent, offset these alterations, thereby preventing excessive manifestations of UVA oxidation-related toxicity. Such response may also be critical to reduce the amount of radiation reaching the deeper layers. On the other hand, the endothelial layer is more susceptible to UVA-induced redox balance disturbance. While being able to adapt quickly to UVA, such response may alter the pump and barrier function of this layer, critical for corneal transparency. Although our results do not allow for the identification of pathways that could be irreversibly disrupted under a chronic exposure, it can be presumed that persistent increases in exogenous ROS will lead to persistent changes in signal transduction or reduce endothelial function efficiency, thus triggering pathological conditions.

Funding info

This work was supported by a grant from the Canadian Institutes of Health Research (CIHR, MOP-133719) to P.J.R.

Conflict of interest

None declared.

Author contributions

Corinne Zinflou: experiment conception and design, analysis and interpretation of data, manuscript writing, and critical revision.

Patrick J Rochette: experiment conception and design, critical revision.

Appendix A. Supporting information

Supplementary data associated with this article can be found in the online version at doi:10.1016/j.freeradbiomed.2017.03.022.

References

[1] J. Dillon, L. Zheng, J.C. Merriam, E.R. Gaillard, The optical properties of the anterior segment of the eye: implications for cortical cataract, Exp. Eye Res. 68 (6) (1999) 785–795, http://dx.doi.org/10.1006/exer.1999.0687.

[2] J.D. Mallet, P.J. Rochette, Ultraviolet light-induced cyclobutane pyrimidine dimers in rabbit eyes, Photochem. Photobiol. 87 (6) (2011) 1363–1368, http://dx.doi.org/10.1111/j.1751-1097.2011.00977.x.

[3] E.A. Boettner, J.R. Wolter, Transmission of the ocular media, Investig. Ophthalmol. Vis. Sci. 1 (6) (1962) 776–783.

[4] H.R. Taylor, S.K. West, F.S. Rosenthal, B. Munoz, H.S. Newland, E.A. Emmett, Corneal changes associated with chronic UV irradiation, Arch. Ophthalmol. 107 (10) (1989) 1481–1484.

[5] R.W. Young, The family of sunlight-related eye diseases, Optom. Vis. Sci. 71 (2) (1994) 125–144.

[6] A.P. Cullen, Photokeratitis and other phototoxic effects on the cornea and conjunctiva, Int. J. Toxicol. 21 (6) (2002) 455–464, http://dx.doi.org/10.1080/10915810290169882.

[7] G. Herrmann, M. Wlaschek, T.S. Lange, K. Prenzel, G. Goerz, K. Scharffetter-Kochanek, UVA irradiation stimulates the synthesis of various matrix-metalloproteinases (MMPs) in cultured human fibroblasts, Exp. Dermatol. 2 (2) (1993) 92–97.

[8] K. Tsukahara, S. Moriwaki, M. Hotta, T. Fujimura, Y. Sugiyama-Nakagiri, S. Sugawara, T. Kitahara, Y. Takema, The effect of sunscreen on skin elastase activity induced by ultraviolet-A irradiation, Biol. Pharm. Bull. 28 (12) (2005) 2302–2307.

[9] Y.Y. He, J. Pi, J.L. Huang, B.A. Diwan, M.P. Waalkes, C.F. Chignell, Chronic UVA irradiation of human HaCaT keratinocytes induces malignant transformation associated with acquired apoptotic resistance, Oncogene 25 (26) (2006) 3680–3688, http://dx.doi.org/10.1038/sj.onc.1209384.

[10] X.X. Huang, F. Bernerd, G.M. Halliday, Ultraviolet A within sunlight induces mutations in the epidermal basal layer of engineered human skin, Am. J. Pathol. 174 (4) (2009) 1534–1543, http://dx.doi.org/10.2353/ajpath.2009.080318.

[11] R. Pastila, S. Heinavaara, L. Ylianttila, D. Leszczynski, In vivo UVA irradiation of mouse is more efficient in promoting pulmonary melanoma metastasis than in vitro, Cancer Cell Int. 11 (1) (2011) 16, http://dx.doi.org/10.1186/1475-2867-11-16.

[12] M.F. Simpanya, R.R. Ansari, V. Leverenz, F.J. Giblin, Measurement of lens protein aggregation in vivo using dynamic light scattering in a guinea pig/UVA model for nuclear cataract, Photochem. Photobiol. 84 (6) (2008) 1589–1595, http://dx.doi.org/10.1111/j.1751-1097.2008.00390.x.

[13] J.P. Liu, R. Schlosser, W.Y. Ma, Z. Dong, H. Feng, L. Lui, X.Q. Huang, Y. Liu, D.W. Li, Human alphaA- and alphaB-crystallins prevent UVA-induced apoptosis through regulation of PKCalpha, RAF/MEK/ERK and AKT signaling pathways, Exp. Eye Res. 79 (6) (2004) 393–403.

[14] S.C. Chao, D.N. Hu, P.Y. Yang, C.Y. Lin, C.W. Nien, S.F. Yang, J.E. Roberts, Ultraviolet-A irradiation upregulated urokinase-type plasminogen activator in pterygium fibroblasts through ERK and JNK pathways, Investig. Ophthalmol. Vis. Sci. 54 (2) (2013) 999–1007, http://dx.doi.org/10.1167/iovs.12-10469.

[15] D. Wu, J. Zhao, D. Wu, J. Zhang, Ultraviolet A exposure induces reversible disruption of gap junction intercellular communication in lens epithelial cells, Int. J. Mol. Med. 28 (2) (2011) 239–245, http://dx.doi.org/10.3892/ijmm.2011.665.

[16] M. Notara, N. Refaian, G. Braun, P. Steven, F. Bock, C. Cursiefen, Short-term ultraviolet A irradiation leads to dysfunction of the limbal niche cells and an antilymphangiogenic and anti-inflammatory micromilieu, Investig. Ophthalmol. Vis. Sci. 57 (3) (2016) 928–939, http://dx.doi.org/10.1167/iovs.15-18343.

[17] L.M. Rapp, A.J. Ghalayini, Influence of UVA light stress on photoreceptor cell metabolism: decreased rates of rhodopsin regeneration and opsin synthesis, Exp. Eye Res. 68 (6) (1999) 757–764, http://dx.doi.org/10.1006/exer.1999.0662.

[18] A. Dovrat, O. Weinreb, Effects of UV-A radiation on lens epithelial NaK-ATPase in organ culture, Investig. Ophthalmol. Vis. Sci. 40 (7) (1999) 1616–1620.

[19] M. Linetsky, V.G. Chemoganskiy, F. Hu, B.J. Ortwerth, Effect of UVA light on the activity of several aged human lens enzymes, Investig. Ophthalmol. Vis. Sci. 44 (1) (2003) 264–274.

[20] F.J. Giblin, V.R. Leverenz, V.A. Padgaonkar, N.J. Unakar, L. Dang, L.R. Lin, M.F. Lou, V.N. Reddy, D. Borchman, J.P. Dillon, UVA light in vivo reaches the nucleus of the guinea pig lens and produces deleterious, oxidative effects, Exp. Eye Res. 75 (4) (2002) 445–458.

[21] A.J. Ridley, J.R. Whiteside, T.J. McMillan, S.L. Allinson, Cellular and sub-cellular responses to UVA in relation to carcinogenesis, Int. J. Radiat. Biol. 85 (3) (2009) 177–195, http://dx.doi.org/10.1080/09553000902740150.

[22] R.M. Tyrrell, S.M. Keyse, New trends in photobiology. The interaction of UVA radiation with cultured cells, J. Photochem. Photobiol. B 4 (4) (1990) 349–361.

[23] T. Polte, R.M. Tyrrell, Involvement of lipid peroxidation and organic peroxides in UVA-induced matrix metalloproteinase-1 expression, Free Radic. Biol. Med. 36 (12) (2004) 1566–1574, http://dx.doi.org/10.1016/j.freeradbiomed.2004.04.003.

[24] S. Zigman, J. Reddan, J.B. Schultz, T. McDaniel, Structural and functional changes in catalase induced by near-UV radiation, Photochem. Photobiol. 63 (6) (1996) 818–824.

[25] D.E. Handy, J. Loscalzo, Redox regulation of mitochondrial function, Antioxid. Redox Signal. 16 (11) (2012) 1323–1367, http://dx.doi.org/10.1089/ars.2011.4123.

[26] J.D. Ly, D.R. Grubb, A. Lawen, The mitochondrial membrane potential (deltapsi (m)) in apoptosis; an update, Apoptosis 8 (2) (2003) 115–128.

[27] K.M. Holmstrom, T. Finkel, Cellular mechanisms and physiological consequences of redox-dependent signalling, Nat. Rev. Mol. Cell Biol. 15 (6) (2014) 411–421, http://dx.doi.org/10.1038/nrm3801.

[28] C. Liu, D. Vojnovic, I.E. Kochevar, U.V. Jurkunas, UV-A Irradiation activates Nrf2-regulated antioxidant defense and induces p53/caspase3-dependent apoptosis in corneal endothelial cells, Investig. Ophthalmol. Vis. Sci. 57 (4) (2016) 2319–2327, http://dx.doi.org/10.1167/iovs.16-19097.

[29] S.P. Gendron, P.J. Rochette, Modifications in stromal extracellular matrix of aged corneas can be induced by ultraviolet A irradiation, Aging Cell 14 (3) (2015) 433–442, http://dx.doi.org/10.1111/acel.12324.

[30] T. Ardan, J. Cejkova, Immunohistochemical expression of matrix metalloproteinases in the rabbit corneal epithelium upon UVA and UVB irradiation, Acta Histochem. 114 (6) (2012) 540–546, http://dx.doi.org/10.1016/j.acthis.2011.10.004.

[31] T. Tsubai, M. Matsuo, Ultraviolet light-induced changes in the glucose-6-phosphate dehydrogenase activity of porcine corneas, Cornea 21 (5) (2002) 495–500.

[32] P.M. Girard, S. Francesconi, D. Graindorge, P.J. Rochette, R. Drouin, E. Sage, UVA-induced damage to DNA and proteins: direct versus indirect photochemical processes, J. Phys: Conf. Ser. 261 (2011) 012002.

[33] Y. Hu, T. Wang, X. Liao, G. Du, J. Chen, J. Xu, Anti-oxidative stress and beyond: multiple functions of the protein glutathionylation, Protein Pept. Lett. 17 (10) (2010) 1234–1244.

[34] B. Chance, B. Schoener, R. Oshino, F. Itshak, Y. Nakase, Oxidation-reduction ratio studies of mitochondria in freeze-trapped samples. NADH and flavoprotein fluorescence signals, J. Biol. Chem. 254 (11) (1979) 4764–4771.

[35] T.S. Blacker, M.R. Duchen, Investigating mitochondrial redox state using NADH and NADPH autofluorescence, Free Radic. Biol. Med. (2016)http://dx.doi.org/10.1016/j.freeradbiomed.2016.08.010.

[36] B. Chance, P. Cohen, F. Jobsis, B. Schoener, Intracellular oxidation-reduction states in vivo, Science 137 (3529) (1962) 499–508.

[37] S.P. Gendron, J.D. Mallet, N. Bastien, P.J. Rochette, Mitochondrial DNA common deletion in the human eye: a relation with corneal aging, Mech. Ageing Dev. 133 (2–3) (2012) 68–74, http://dx.doi.org/10.1016/j.mad.2012.01.002.

[38] Z. Karabekian, N.D. Gillum, E.W. Wong, N. Sarvazyan, Effects of N-cadherin overexpression on the adhesion properties of embryonic stem cells, Cell Adhes Migr. 3 (3) (2009) 305–310.
[39] W.E. Kurtin, J.A. Zuclich, Action spectrum for oxygen-dependent near-ultraviolet induced corneal damage, Photochem. Photobiol. 27 (3) (1978) 329–333.
[40] I. Dalle-Donne, R. Rossi, G. Colombo, D. Giustarini, A. Milzani, Protein S-glutathionylation: a regulatory device from bacteria to humans, Trends Biochem. Sci. 34 (2) (2009) 85–96, http://dx.doi.org/10.1016/j.tibs.2008.11.002.
[41] P. Klatt, S. Lamas, Regulation of protein function by S-glutathiolation in response to oxidative and nitrosative stress, Eur. J. Biochem. 267 (16) (2000) 4928–4944.
[42] D. Graindorge, S. Martineau, C. Machon, P. Arnoux, J. Guitton, S. Francesconi, C. Frochot, E. Sage, P.M. Girard, Singlet Oxygen-mediated oxidation during UVA radiation alters the dynamic of genomic DNA replication, PLoS One 10 (10) (2015) e0140645, http://dx.doi.org/10.1371/journal.pone.0140645.
[43] C. Hwang, A.J. Sinskey, H.F. Lodish, Oxidized redox state of glutathione in the endoplasmic reticulum, Science 257 (5076) (1992) 1496–1502.
[44] M. Demasi, G.M. Silva, L.E. Netto, 20 S proteasome from Saccharomyces cerevisiae is responsive to redox modifications and is S-glutathionylated, J. Biol. Chem. 278 (1) (2003) 679–685, http://dx.doi.org/10.1074/jbc.M209282200.
[45] M. Fratelli, H. Demol, M. Puype, S. Casagrande, I. Eberini, M. Salmona, V. Bonetto, M. Mengozzi, F. Duffieux, E. Miclet, A. Bachi, J. Vandekerckhove, E. Gianazza, P. Ghezzi, Identification by redox proteomics of glutathionylated proteins in oxidatively stressed human T lymphocytes, Proc. Natl. Acad. Sci. USA 99 (6) (2002) 3505–3510, http://dx.doi.org/10.1073/pnas.052592699.
[46] L. Kolozsvari, A. Nogradi, B. Hopp, Z. Bor, UV absorbance of the human cornea in the 240- to 400-nm range, Invest Ophthalmol. Vis. Sci. 43 (7) (2002) 2165–2168.
[47] W. Ying, NAD+/NADH and NADP+/NADPH in cellular functions and cell death: regulation and biological consequences, Antioxid. Redox Signal. 10 (2) (2008) 179–206, http://dx.doi.org/10.1089/ars.2007.1672.
[48] K. Blinova, S. Carroll, S. Bose, A.V. Smirnov, J.J. Harvey, J.R. Knutson, R.S. Balaban, Distribution of mitochondrial NADH fluorescence lifetimes: steady-state kinetics of matrix NADH interactions, Biochemistry 44 (7) (2005) 2585–2594, http://dx.doi.org/10.1021/bi0485124.
[49] M.C. Skala, K.M. Riching, A. Gendron-Fitzpatrick, J. Eickhoff, K.W. Eliceiri, J.G. White, N. Ramanujam, In vivo multiphoton microscopy of NADH and FAD redox states, fluorescence lifetimes, and cellular morphology in precancerous epithelia, Proc. Natl. Acad. Sci. USA 104 (49) (2007) 19494–19499, http://dx.doi.org/10.1073/pnas.0708425104.
[50] M. Reim, E. Weidenfeld, A.W. Budi Santoso, Oxidized and reduced glutathione levels of the cornea in vivo, Albrecht Von Graefes Arch. Klin Exp. Ophthalmol. 211 (2) (1979) 165–175.
[51] M. Fratelli, H. Demol, M. Puype, S. Casagrande, P. Villa, I. Eberini, J. Vandekerckhove, E. Gianazza, P. Ghezzi, Identification of proteins undergoing glutathionylation in oxidatively stressed hepatocytes and hepatoma cells, Proteomics 3 (7) (2003) 1154–1161, http://dx.doi.org/10.1002/pmic.200300436.
[52] M. Lombardo, G. Pucci, R. Barberi, G. Lombardo, Interaction of ultraviolet light with the cornea: clinical implications for corneal crosslinking, J. Cataract Refract. Surg. 41 (2) (2015) 446–459, http://dx.doi.org/10.1016/j.jcrs.2014.12.013.
[53] S.P. Gendron, N. Bastien, J.D. Mallet, P.J. Rochette, The 3895-bp mitochondrial DNA deletion in the human eye: a potential involvement in corneal ageing and macular degeneration, Mutagenesis 28 (2) (2013) 197–204, http://dx.doi.org/10.1093/mutage/ges071.
[54] J.A. Bonanno, Molecular mechanisms underlying the corneal endothelial pump, Exp. Eye Res. 95 (1) (2012) 2–7, http://dx.doi.org/10.1016/j.exer.2011.06.004.
[55] M. Nakamura, T. Nakano, M. Hikida, Effects of oxidized glutathione and reduced glutathione on the barrier function of the corneal endothelium, Cornea 13 (6) (1994) 493–495.
[56] M.C. Ng, M.V. Riley, Relation of intracellular levels and redox state of glutathione to endothelial function in the rabbit cornea, Exp. Eye Res. 30 (5) (1980) 511–517.
[57] S.L. Bonting, K.A. Simon, N.M. Hawkins, Studies on sodium-potassium-activated adenosine triphosphatase. I. Quantitative distribution in several tissues of the cat, Arch. Biochem. Biophys. 95 (1961) 416–423.
[58] M.V. Riley, A role for glutathione and glutathione reductase in control of corneal hydration, Exp. Eye Res. 39 (6) (1984) 751–758.
[59] U.V. Jurkunas, M.S. Bitar, T. Funaki, B. Azizi, Evidence of oxidative stress in the pathogenesis of fuchs endothelial corneal dystrophy, Am. J. Pathol. 177 (5) (2010) 2278–2289, http://dx.doi.org/10.2353/ajpath.2010.100279.